Electronic Supplementary Information

Multifunctional dielectric/optical response with broadband white light emission in hybrid stannic halide crystal

Qing-Feng Luo, Hao-Fei Ni, Pei-Zhi Huang, Ming Zhu, Chang-Feng Wang, Qian-Hao Zhuo, Da-Wei Fu,* Yi Zhang* and Zhi-Xu Zhang*

Institute for Science and Applications of Molecular Ferroelectrics, Key Laboratory of the Ministry of Education for Advanced Catalysis Materials, Zhejiang Normal University, Jinhua, 321004, People's Republic of China

E-mail: dawei@zjnu.edu.cn, yizhang1980@seu.edu.cn, zhangzhixu@zjnu.edu.cn

Experimental Section

X-ray single crystal diffraction (SC-XRD)

All single-crystal X-ray diffraction data in the work were collected by using a Bruker D8 APEX-III diffractometer with Mo-Kα radiation (λ = 0.71073 Å) (operating at 50 kV and 1.4 mA). Data reduction and numerical absorption corrections were generated using APEX-III software. Refinement of single crystal data were solved and refined using SHELXT and OLEX 1.5 software packages, all non-hydrogen atoms are anisotropically manipulated. The drawing of $(TMPA)_2SnCl_6$ and $(TMPA)_2SnBr_6$ were described using DIAMOND software. The crystal data (CCDC number: 2174141, 2174142 and 2242964.) have been uploaded to the Crystallography data center in Cambridge (CCDC) in the work.

Dielectric measurements

Crystals were ground into powder, and the appropriate amount was prepared into round flakes of 0.6 mm thickness. The process was carried out in a particular mold under a pressure of 50 MPa. In the next step, a knife cut the circular sheet into 3 × 4 mm^2 small pieces. Then, a simple capacitor was prepared by taking 8 mm copper wire and silver glue to fix the small sheet on the electrode holders. Finally, the electrodes were connected to the Tonghui TH2828A instrument, and the dielectric constant was tested at frequencies

ranging from 500 Hz to 1 MHz with 1 V AC voltage. All the above preparation processes were carried out in an air environment.

Thermal and phase stabilities

NETZSCH DSC 214 instrument was used for differential scanning calorimetry (DSC) measurement. Crystals were ground into powder. The powder sample with a mass of about 10 mg was weighed with an analytical balance and placed in an aluminum crucible. In the next step, the aluminum lid pokes a small hole with an iron pin, and the crucible is sealed with a press. Finally, heating and cooling cycles were measured at a rate of 20 K min^{-1} in the range of 290-410 K under a nitrogen atmosphere. Thermogravimetric analysis (TGA) was performed on the NETZSCH STA449 F5 instrument. Crystals were ground into powder. The powder sample with a mass of about 10mg was weighed with an analytical balance and placed in a crucible. In the next step, the crucible is covered with the matching crucible lid and put onto the instrument. Finally, Thermogravimetric analysis (TGA) was performed in the temperature range of 373 to 1073 K at a heating rate of 10 K min^{-1} under an air atmosphere.

Powder X-ray diffraction

Powder X-ray diffraction (PXRD) data for two compounds were measured on a D8 Advance 03030502 instrument at room temperature. Diffraction patterns were collected in the 2θ range of 5~50° with a step size of 0.02°.

UV-Vis Measurements

UV-near-infrared-visible (UV-NIR-vis) spectra were obtained on a Cary RF 6000 instrument. The UV spectrum was tested in the range of 200 nm-800 nm with a step size of 1 nm.

Fluorescence Spectrofluorometer

The emission and excitation spectra of samples were measured using an Edinburgh FLS1000 fluorescence spectrophotometer equipped with a xenon lamp as the excitation source, and time-resolved spectra were recorded through the Edinburgh spectrophotometer equipped with a microsecond pulsed hydrogen lamp. The photoluminescence quantum efficiency of compounds was characterized using an integrating sphere in the spectrofluorometer. The CIE chromaticity coordinates were calculated using the CIE 1931 software package based on the emission spectrum data .The PLQEs were calculated by the equation:

$\eta_{QE} = I_S /(E_R - E_S)$, in which I_S represents the luminescence emission spectrum of $(TMPA)_2SnCl_6$, E_R is the spectrum of the excitation light from the empty integrated sphere (without the sample), and E_S is the excitation spectrum for $(TMPA)_2SnCl_6$ exciting.

Calculation of the *ΔS* compounds in the heating and cooling cycles

$(TMPA)_2SnCl_6$ is ΔS_1 in the heating cycle

$$\Delta S_1 = \int_{T_1}^{T_0} \frac{Q}{T} dT \approx \frac{\Delta H}{T_P}$$

$$= \frac{56.72\ J \cdot g^{-1} \times 511.68\ g \cdot mol^{-1}}{391.3\ K}$$

$$= 74.17\ J \cdot mol^{-1} \cdot K^{-1}$$

$(TMPA)_2SnCl_6$ is ΔS_2 in the cooling cycle

$$\Delta S_2 = \int_{T_2}^{T_0} \frac{Q}{T} dT \approx \frac{\Delta H}{T_P}$$

$$= \frac{49.32\ J \cdot g^{-1} \times 511.68\ g \cdot mol^{-1}}{328.9\ K}$$

$$= 76.73\ J \cdot mol^{-1} \cdot K^{-1}$$

$$\Delta S_{ave} = \frac{\Delta S_2 + \Delta S_1}{2} = \frac{76.73\ J \cdot mol^{-1} \cdot K^{-1} + 74.17\ J \cdot mol^{-1} \cdot K^{-1}}{2} = 75.45\ J \cdot mol^{-1} \cdot K^{-1}$$

$(TMPA)_2SnBr_6$ is ΔS_3 in the heating cycle

$$\Delta S_3 = \int_{T_3}^{T_0} \frac{Q}{T} dT \approx \frac{\Delta H}{T_P}$$

$$= \frac{24.49\ J \cdot g^{-1} \times 778.44\ g \cdot mol^{-1}}{374.7\ K}$$

$$= 50.88\ J \cdot mol^{-1} \cdot K^{-1}$$

$(TMPA)_2SnBr_6$ is ΔS_4 in the cooling cycle

$$\Delta S_4 = \int_{T_4}^{T_0} \frac{Q}{T} dT \approx \frac{\Delta H}{T_P}$$

$$= \frac{22.71\ J \cdot g^{-1} \times 778.44\ g \cdot mol^{-1}}{361.3\ K}$$

$$= 48.93\ J \cdot mol^{-1} \cdot K^{-1}$$

$$\Delta S_{ave} = \frac{\Delta S_4 + \Delta S_3}{2} = \frac{48.93\ J \cdot mol^{-1} \cdot K^{-1} + 50.88\ J \cdot mol^{-1} \cdot K^{-1}}{2} = 49.90\ J \cdot mol^{-1} \cdot K^{-1}$$

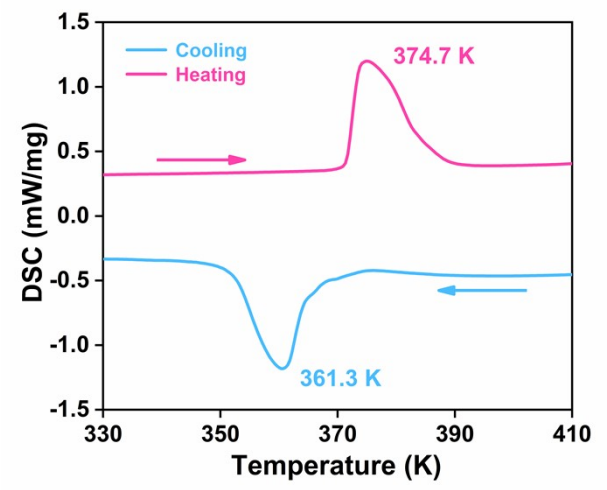

Fig. S1 DSC curve of $(TMPA)_2SnBr_6$ in heating-cooling runs.

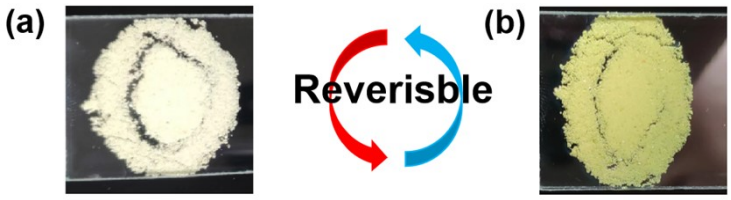

Fig. S2 (a) $(TMPA)_2SnBr_6$ powder color at low temperature. (b) $(TMPA)_2SnBr_6$ powder color at high temperature.

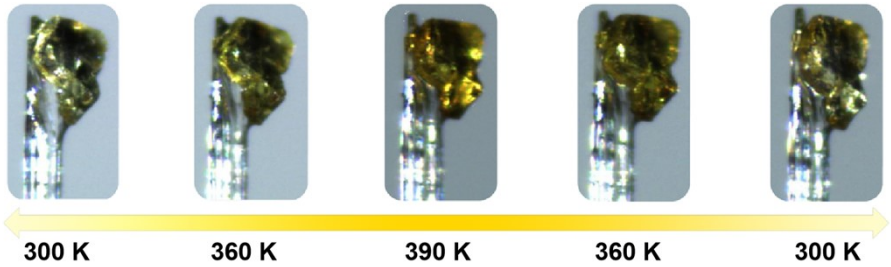

Fig. S3 Temperature-induced color change in the $(TMPA)_2SnBr_6$ crystal for heating-cooling cycle.

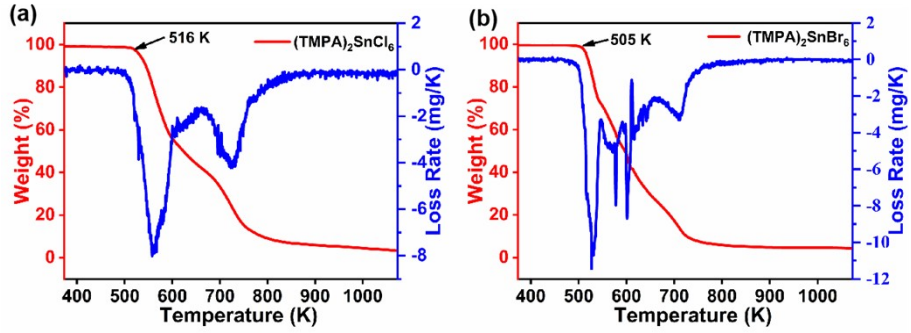

Fig. S4 (a) TG and DTG of $(TMPA)_2SnCl_6$ from 373 K to 1073 K. (b) TG and DTG of $(TMPA)_2SnBr_6$ of $(TMPA)_2SnBr_6$ from 373 K to 1073 K.

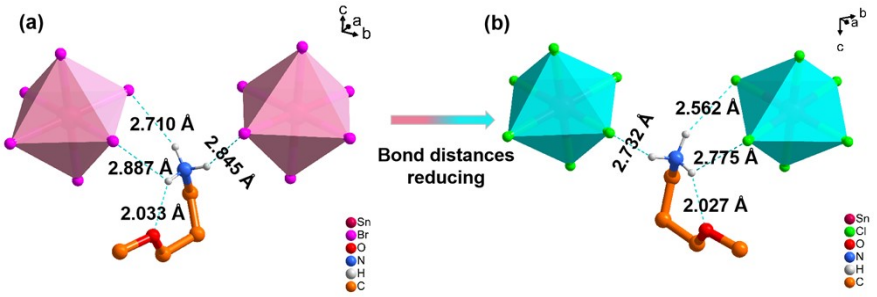

Fig. S5 (a) Intermolecular interaction microstructure of $(TMPA)_2SnCl_6$ at 300 K. (b) Intermolecular interaction microstructure of $(TMPA)_2SnBr_6$ at 300 K.

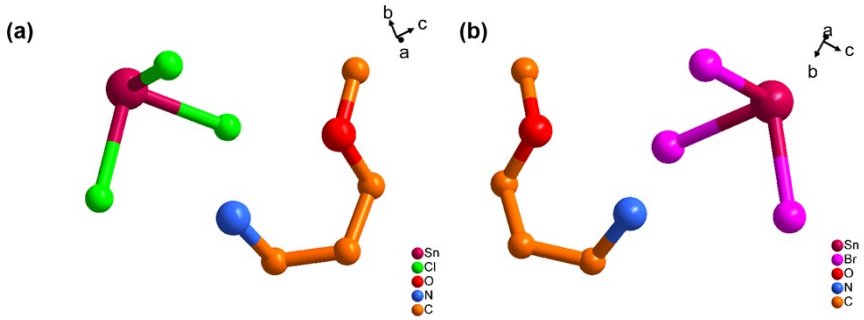

Fig. S6 (a)The asymmetric unit structure of $(TMPA)_2SnCl_6$. (b) The asymmetric unit structure of $(TMPA)_2SnBr_6$.

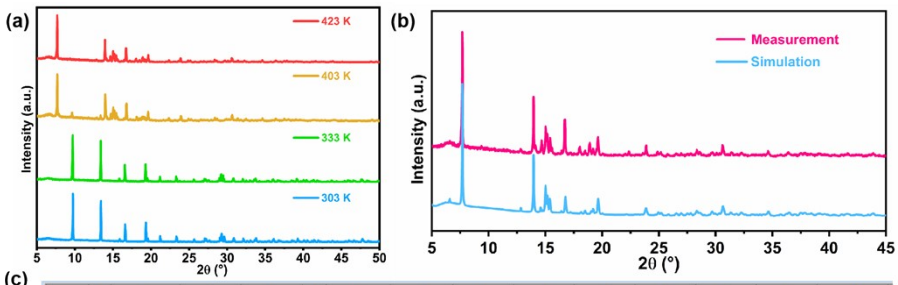

(c)

#	FOM	Rwp	Space Group	IT #	Option	System	a	b	c	alpha	beta	gamma	Volume
1	17.82167319	17.54338545	PCMN	62	Origin-1,-cba	Orthorhombic	19.42999000	14.26884000	13.42411000	90.00000000	90.00000000	90.00000000	3.721746e+003
2	17.82167319	17.54338545	PC21N	33	Origin-1,bca	Orthorhombic	19.42999000	14.26884000	13.42411000	90.00000000	90.00000000	90.00000000	3.721746e+003
3	16.83897466	17.45374182	PB2N	30	Origin-1,bca	Orthorhombic	19.42999000	14.26884000	13.42411000	90.00000000	90.00000000	90.00000000	3.721746e+003
4	16.83897466	17.45374182	PBMN	53	Origin-1,-c-ab	Orthorhombic	19.42999000	14.26884000	13.42411000	90.00000000	90.00000000	90.00000000	3.721746e+003
5	15.42654276	18.85855105	PBCN	60	Origin-1	Orthorhombic	19.42999000	14.26884000	13.42411000	90.00000000	90.00000000	90.00000000	3.721746e+003
6	15.36379636	17.59849649	PN2N	34	Origin-1,a-cb	Orthorhombic	19.42999000	14.26884000	13.42411000	90.00000000	90.00000000	90.00000000	3.721746e+003
7	15.36379636	17.59849649	PNMN	58	Origin-1,a-cb	Orthorhombic	19.42999000	14.26884000	13.42411000	90.00000000	90.00000000	90.00000000	3.721746e+003

Fig. S7 (a) The temperature Dependent Powder X-ray Diffraction of $(TMPA)_2SnCl_6$. (b) Pawley refinement of PXRD data of $(TMPA)_2SnCl_6$ collected at 423 K with a Orthorhombic unit cell. (c) High temperature structure simulation of $(TMPA)_2SnCl_6$.

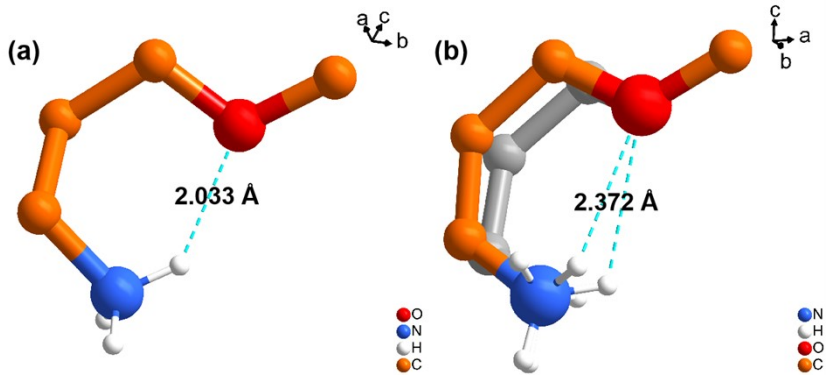

Fig. S8 (a) The intramolecular hydrogen bonding force distance of $(TMPA)_2SnBr_6$ at 300 K. (b) The intramolecular hydrogen bonding force distance of $(TMPA)_2SnBr_6$ at 380 K.

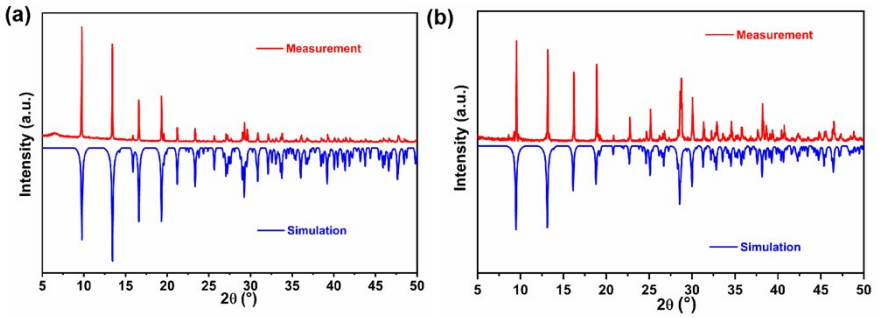

Fig. S9 (a) Powder X-ray diffraction (PXRD) for $(TMPA)_2SnCl_6$. (b) Powder X-ray diffraction (PXRD) for $(TMPA)_2SnBr_6$.

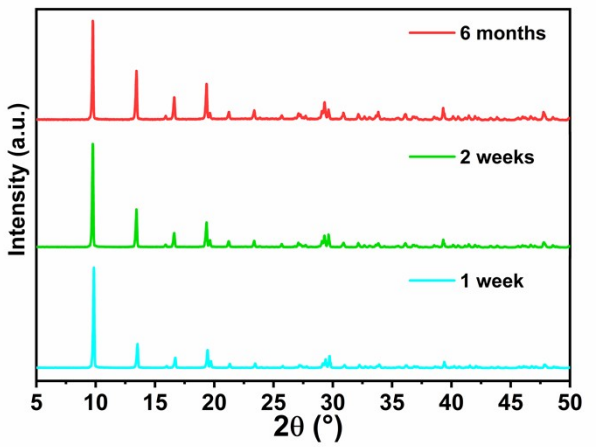

Fig. S10 Powder X-ray Diffraction of $(TMPA)_2SnCl_6$ at different times.

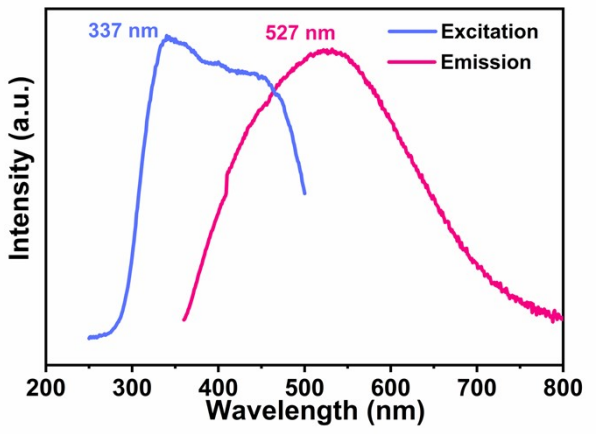

Fig. S11 Excitation and emission spectra for $(TMPA)_2SnCl_6$.

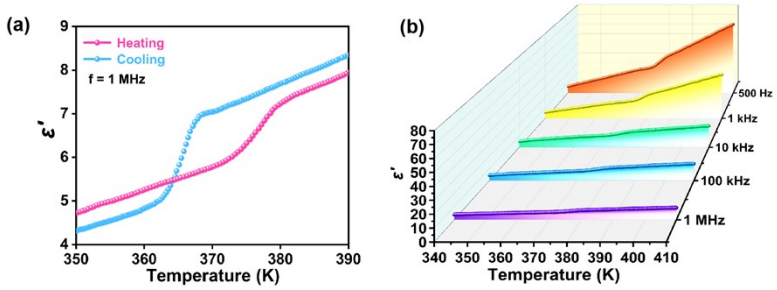

Fig. S12 (a) Dielectric constant of $(TMPA)_2SnBr_6$. (b) Temperature dependence of the real part (ε′) of $(TMPA)_2SnBr_6$ at different frequencies in the heating run.

Table S1. Crystallographic data and structural refinement details of $(TMPA)_2SnCl_6$ and $(TMPA)_2SnBr_6$.

Compound	$(TMPA)_2SnCl_6$	$(TMPA)_2SnBr_6$	
	LTP	LTP	HTP
CCDC Code	2174142	2174141	2242964
Formula	$C_8H_{24}Cl_6N_2O_2Sn$	$C_8H_{24}Br_6N_2O_2Sn$	$C_8H_{24}Br_6N_2O_2Sn$
Fw	511.68	778.44	778.44
Temp(K)	300	300	380
Crystal Syst	Orthorhombic	Orthorhombic	Orthorhombic
Space group	*Pbca*	*Pbca*	*Pnma*
a(Å)	8.3736 (15)	8.5371 (13)	13.759 (8)
b(Å)	13.195 (3)	13.561 (2)	8.011 (4)
c(Å)	18.117 (4)	18.663	19.750 (11)
α/°	90	90	90
β/°	90	90	90
γ/°	90	90	90
V(Å^3)	2001.8 (7)	2160.6 (6)	2177 (2)
Z	4	4	4
μ(mm^{-1})	2.08	12.28	12.19
GOF on F^2	1.034	1.162	1.164
R_1[[I > 2σ(I)]	0.025	0.0312	0.0583
wR_2 (all data)	0.055	0.0806	0.1626

Table S2. Selected bond lengths /Å and angles/° for $(TMPA)_2SnBr_6$ and $(TMPA)_2SnCl_6$ at 300 K.

Temperature at 300 K			
$(TMPA)_2SnBr_6$		$(TMPA)_2SnCl_6$	
Sn1—Br3i	2.5857 (5)	Sn1—Cl1	2.4200 (8)
Sn1—Br3	2.5857 (6)	Sn1—Cl1i	2.4201 (8)
Sn1—Br2	2.6175 (6)	Sn1—Cl3	2.4566 (8)
Sn1—Br2i	2.6175 (6)	Sn1—Cl3i	2.4566 (8)
Sn1—Br1i	2.6019 (6)	Sn1—Cl2i	2.4355 (8)
Sn1—Br1	2.6019 (6)	Sn1—Cl2	2.4355 (8)
Br3i—Sn1—Br3	180.0	Cl1—Sn1—Cl1i	180.0
Br3—Sn1—Br2i	88.27 (2)	Cl1—Sn1—Cl3	91.76 (3)
Br3i—Sn1—Br2	88.27 (2)	Cl1i—Sn1—Cl3	88.25 (3)
Br3i—Sn1—Br2i	91.73 (2)	Cl1—Sn1—Cl3i	88.24 (3)
Br3—Sn1—Br2	91.73 (2)	Cl1i—Sn1—Cl3i	91.75 (3)
Br3i—Sn1—Br1i	90.82 (2)	Cl1—Sn1—Cl2i	89.34 (3)
Br3i—Sn1—Br1	89.18 (2)	Cl1—Sn1—Cl2	90.66 (3)
Br3—Sn1—Br1	90.82 (2)	Cl1i—Sn1—Cl2i	90.66 (3)
Br3—Sn1—Br1i	89.18 (2)	Cl1i—Sn1—Cl2	89.34 (3)
Br2i—Sn1—Br2	180.00 (2)	Cl3i—Sn1—Cl3	180.0
Br1i—Sn1—Br2	90.44 (2)	Cl2i—Sn1—Cl3	90.57 (3)
Br1i—Sn1—Br2i	89.56 (2)	Cl2i—Sn1—Cl3i	89.43 (3)
Br1—Sn1—Br2i	90.44 (2)	Cl2—Sn1—Cl3i	90.58 (3)
Br1—Sn1—Br2	89.56 (2)	Cl2—Sn1—Cl3	89.42 (3)
Br1i—Sn1—Br1	180.0	Cl2i—Sn1—Cl2	180.0

Symmetry code: (i) −x+31, −y+1, −z+1.

Table S3. Selected bond lengths /Å and angles/° for $(TMPA)_2SnBr_6$ at 380 K.

$(TMPA)_2SnBr_6$			
bond lengths /Å		bond angles/°	
Sn1—Br4	2.5777 (19)	Br4—Sn1—Br4i	91.29 (10)
Sn1—Br4i	2.5777 (19)	Br4—Sn1—Br3	91.67 (8)
Sn1—Br3	2.586 (3)	Br4i—Sn1—Br3	91.67 (8)
Sn1—Br2i	2.597 (2)	Br4—Sn1—Br2	179.41 (8)
Sn1—Br2	2.597 (2)	Br4i—Sn1—Br2i	179.41 (8)
Sn1—Br1	2.579 (3)	Br4i—Sn1—Br2	88.99 (7)
		Br4—Sn1—Br2i	89.00 (7)
		Br4i—Sn1—Br1	89.85 (8)
		Br4—Sn1—Br1	89.85 (8)
		Br3—Sn1—Br2i	87.80 (8)
		Br3—Sn1—Br2	87.80 (8)
		Br2—Sn1—Br2i	90.71 (10)
		Br1—Sn1—Br3	177.82 (11)
		Br1—Sn1—Br2i	90.67 (8)
		Br1—Sn1—Br2	90.67 (8)

Symmetry codes: (i) x, −y−1/2, z; (ii) x, −y+1/2, z; (iii) x, −y+3/2, z.

Table S4. Hydrogen-bond geometry (Å, °) for $(TMPA)_2SnCl_6$ at 300 K.

D—H···A	D—H	H···A	D···A	D—H···A
N1—H1A···Cl3ii	0.89	2.72	3.499 (3)	146
N1—H1A···Cl2ii	0.89	2.90	3.611 (3)	138
N1—H1B···Cl3i	0.89	2.56	3.408 (3)	159
N1—H1C···Cl2	0.89	2.77	3.347 (3)	123
N1—H1C···O1	0.89	2.03	2.735 (3)	135
C2—H2B···Cl1iii	0.97	2.97	3.782 (3)	142
C1—H1D···Cl3iii	0.97	2.95	3.724 (3)	138

Symmetry codes: (i) −x+1, −y+1, −z+1; (ii) −x+1/2, y−1/2, z; (iii) −x+3/2, y−1/2, z.

Table S5. Hydrogen-bond geometry (Å, °) for $(TMPA)_2SnBr_6$ at 300 K.

D—H···A	D—H	H···A	D···A	D—H···A
N1—H1A···Br2i	0.89	2.71	3.572 (5)	163
N1—H1B···Br1	0.89	2.88	3.451 (4)	124
N1—H1B···O1	0.89	2.03	2.746 (6)	136
N1—H1C···Br2ii	0.89	2.85	3.612 (5)	145
C1—H1D···Br2iii	0.97	2.98	3.791 (5)	142
C4—H4A···Br3iii	0.97	3.09	3.871 (6)	139

Table S6. Hydrogen-bond geometry (Å, °) for $(TMPA)_2SnBr_6$ at 380 K.

D—H···A	D—H	H···A	D···A	D—H···A
N2—H2C···Br4iv	0.89	3.08	3.646 (19)	123
N2—H2C···Br4i	0.89	2.97	3.646 (19)	134
N2—H2B···Br2ii	0.89	3.04	3.557 (18)	119
N2—H2A···Br2	0.89	2.72	3.557 (18)	157

N1—H1B···Br2v	0.89	2.83	3.53 (2)	137
N1—H1B···O1	0.89	2.21	2.81 (3)	125
N1—H1C···Br2vi	0.89	3.01	3.53 (2)	119
N1—H1C···Br2vii	0.89	3.02	3.705 (19)	135
N1—H1A···Br2viii	0.89	2.84	3.705 (19)	164
C7—H7B···Br3ix	1.01	3.01	3.91 (3)	150
C5—H5A···Br4x	0.87	3.14	3.97 (4)	162
C5—H5A···Br4xi	0.87	3.14	3.64 (4)	119
C5—H5B···Br1	0.97	2.88	3.76 (5)	152
C1—H1D···Br3ix	0.97	2.96	3.86 (6)	154
C1—H1E···Br4ix	0.96	3.03	3.63 (4)	121
C1—H1E···Br4xii	0.96	3.03	3.88 (5)	148

Symmetry codes: (i) x, −y−1/2, z; (ii) x, −y+1/2, z; (iv) x, y+1, z; (v) x−1/2, y+1, −z+3/2; (vi) x−1/2, −y+1/2, −z+3/2; (vii) −x+1/2, y+1/2, z+1/2; (viii) −x+1/2, −y+1, z+1/2; (ix) −x+1/2, −y, z+1/2; (x) −x, −y, −z+1; (xi) −x, y+1/2, −z+1; (xii) −x+1/2, y+3/2, z+1/2.

Table S7. The void volume of $(TMPA)_2SnCl_6$ and $(TMPA)_2SnBr_6$ at 300 K. ($V_{void} = V_{cell} - 4V_{octahedron}$). There are four completed octahedrons in a unit cell and the octahedron volume was calculated by DIAMOND software.

	$(TMPA)_2SnCl_6$	$(TMPA)_2SnBr_6$
Cell volume (Å^3)	2001.8	2160.6
Octahedron volume (Å^3)	19.3	23.4
Void volume (Å^3)	1924.6	2067

Table S8. The CCT, CIE and CRI of organic-inorganic hybrid materials with white emission

Compound	CCR	CIE	CRI	Ref
TJU-3	5620	(0.33, 0.41)	78	1
$C_5N_2H_{14}SnCl_4$	4168	(0.39, 0.43)	80	2
$(DTHPE)_2Pb_3Cl_{10}$	14300	(0.25, 0.29)	81	3
$PPASnCl_6$:3.5%Sb	5863	(0.32, 0.34)	84	4
$(C_4H_9NH_3)_2$ $PbCl_4$	4423	(0.37, 0.40)	86	5
$(C_6H_5C_2H_4NH_3)_2PbBr_{2.5}Cl_{1.5}$	9786	(0.28, 0.29)	91	6
PEPC-3N	5500	(0.33, 0.36)	78	7
PEPC-NIA5	5322	(0.34, 0.37)	75	8
(N-MEDA) $PbBr_4$	6502	(0.31, 0.36)	85	9
$(DMEN)PbBr_4$	7843	(0.28, 0.36)	73	10
$(DTHPE)_{0.5}PbCl_3$	9423	(0.27, 0.32)	83	11
$(DMTHP)PbCl_3$	7344	(0.29, 0.37)	76	11
$(DBN)PbCl_3$	13686	(0.25, 0.29)	82	11
$(TAE)_2[Pb_2Cl_{10}]$ $(Cl)_2$	6741	(0.30, 0.33)	96	12
$(HMEDA)CdBr_2$	10536	(0.26, 0.31)	83	13
$(C_8NH_{12})_6InBr_9·H_2O$:1%Sb	3347	(0.40, 0.36)	84	14
$C_6H_{12}N_3PbCl_4$	4203	(0.36, 0.37)	93	15
(4amp) $PbBr_4$	6275	(0.31, 0.39)	76	16
$(TMPA)_2SnCl_6$ (This work)	5390	(0.31, 0.35)	86.7	

Reference

1. Z. Zhuang, C. Peng, G. Zhang, H. Yang, J. Yin and H. Fei, Intrinsic Broadband White-Light Emission from Ultrastable, Cationic Lead Halide Layered Materials, *Angew. Chem. Int. Ed.*, 2017, **56**, 14411-14416.
2. G. Song, Z. Li, P. Gong, R. J. Xie and Z. Lin, Tunable White Light Emission in a Zero-Dimensional Organic–Inorganic Metal Halide Hybrid with Ultra-High Color Rendering Index, *Adv. Opt. Mater.*, 2021, **9**, 2002246.
3. J. Q. Zhao, C. Sun, M. Yue, Y. Meng, X. M. Zhao, L. R. Zeng, G. Chen, C. Y. Yue and X. W. Lei, Lead chlorine cluster assembled one-dimensional halide with highly efficient broadband white-light emission, *Chem. Commun.*, 2021, **57**, 1218-1221.
4. G. Zhang, P. Dang, H. Xiao, H. Lian, S. Liang, L. Yang, Z. Cheng, G. Li and J. Lin, Antimony-Doped Lead-Free Zero-Dimensional Tin(IV)-Based Organic–Inorganic Metal Halide Hybrids with High Photoluminescence Quantum Yield and Remarkable Stability, *Adv. Opt. Mater.*, 2021, **9**, 2101637.
5. C. Ji, S. Wang, L. Li, Z. Sun, M. Hong and J. Luo, The First 2D Hybrid Perovskite Ferroelectric Showing Broadband White-Light Emission with High Color Rendering Index, *Adv. Funct. Mater.*, 2018, **29**, 1805038.
6. S. Yang, Z. Lin, J. Wang, Y. Chen, Z. Liu, E. Yang, J. Zhang and Q. Ling, High Color Rendering Index White-Light Emission from UV-Driven LEDs Based on Single Luminescent Materials: Two-Dimensional Perovskites $(C_6H_5C_2H_4NH_3)_2PbBr_xCl_{4-x}$, *ACS Appl. Mater. Interfaces.*, 2018, **10**, 15980-15987.
7. Q. Huang, S. Yang, S. Feng, H. Zhen, Z. Lin and Q. Ling, Multicolor Output from 2D Hybrid Perovskites with Wide Band Gap: Highly Efficient White Emission, Dual-Color Afterglow, and Switch between Fluorescence and Phosphorescence, *J. Phys. Chem. Lett.*, 2021, **12**, 1040-1045.
8. S. Yang, D. Wu, W. Gong, Q. Huang, H. Zhen, Q. Ling and Z. Lin, Highly efficient room-temperature phosphorescence and afterglow luminescence from common organic fluorophores in 2D hybrid perovskites, *Chem. Sci.*, 2018, **9**, 8975-8981.
9. E. R. Dohner, E. T. Hoke and H. I. Karunadasa, Self-assembly of broadband white-light emitters, *J. Am. Chem. Soc.*, 2014, **136**, 1718-1721.

10. L. Mao, Y. Wu, C. C. Stoumpos, M. R. Wasielewski and M. G. Kanatzidis, White-Light Emission and Structural Distortion in New Corrugated Two-Dimensional Lead Bromide Perovskites, *J. Am. Chem. Soc.*, 2017, **139**, 5210-5215.

11. W. F. Zhang, W. J. Pan, T. Xu, R. Y. Song, Y. Y. Zhao, C. Y. Yue and X. W. Lei, One-Dimensional Face-Shared Perovskites with Broad-Band Bluish White-Light Emissions, *Inorg. Chem.*, 2020, **59**, 14085-14092.

12. S. Elleuch, A. Lusson, S. Pillet, K. Boukheddaden and Y. Abid, White Light Emission from a Zero-Dimensional Lead Chloride Hybrid Material, *ACS Photonics.*, 2020, **7**, 1178-1187.

13. C. Sun, W. L. He, M. J. Liu, W. J. Pan, L. F. Dong, G. Chen, G. D. Liu and X. W. Lei, Zero-Dimensional Hybrid Cd-Based Perovskites with Broadband Bluish White-Light Emissions, *Chem.-Asian J.*, 2020, **15**, 3050-3058.

14. Z. Li, G. Song, Y. Li, L. Wang, T. Zhou, Z. Lin and R. J. Xie, Realizing Tunable White Light Emission in Lead-Free Indium(III) Bromine Hybrid Single Crystals through Antimony(III) Cation Doping, *J. Phys. Chem. Lett.*, 2020, **11**, 10164-10172.

15. Z. Wu, C. Ji, Z. Sun, S. Wang, S. Zhao, W. Zhang, L. Li and J. Luo, Broadband white-light emission with a high color rendering index in a two-dimensional organic–inorganic hybrid perovskite, *J. Mater. Chem. C.*, 2018, **6**, 1171-1175.

16. L. Mao, P. Guo, M. Kepenekian, I. Hadar, C. Katan, J. Even, R. D. Schaller, C. C. Stoumpos and M. G. Kanatzidis, Structural Diversity in White-Light-Emitting Hybrid Lead Bromide Perovskites, *J. Am. Chem. Soc.*, 2018, **140**, 13078-13088.